GEOPHYSICS, VOL. 71, NO. 6 (NOVEMBER-DECEMBER 2006); P. D191–D202, 15 FIGS., 1 TABLE.
10.1190/1.2358402

Elastic-wave propagation in deviated wells in anisotropic formations

Bikash K. Sinha[1], Ergün Şimşek[2], and Qing-Huo Liu[2]

ABSTRACT

A finite-difference time-domain (FDTD) formulation with perfectly matched layer (PML) enables analysis of elastic-wave propagation in a fluid-filled borehole in an arbitrarily anisotropic formation. The FDTD formulation yields synthetic waveforms at an array of receivers produced by a monopole or dipole source placed on the borehole axis. Synthetic waveforms are then processed by a modified matrix pencil algorithm to isolate both nondispersive and dispersive arrivals in the wavetrain. The processing algorithm used in this study extracts phase slownesses of plane waves that agree well with the corresponding phase slownesses calculated for propagation along an arbitrary direction in an anisotropic formation. The tube-wave phase velocity obtained from the zero-frequency intercept of the Stoneley dispersion compares well with the analytical results for deviated wellbores in both fast and slow transversely isotropic (TI) formations. Good agreement is also obtained between the low-frequency asymptotes of borehole flexural dispersion and the corresponding shear-wave velocities from a numerically exact solution of Kelvin-Christoffel equations for plane-wave velocities in anisotropic formations. Numerical results indicate that the Stoneley dispersion changes by a rather small amount, whereas the dipole flexural dispersions exhibit larger changes with wellbore deviations. The influence of a sonic tool structure on borehole elastic-waves can be described by an equivalent heavy-fluid column placed concentrically with the borehole axis. The effect of a heavy-fluid column on the borehole flexural mode is larger in fast than in slow formations. However, the Stoneley dispersion at low frequencies is affected by the presence of the tool structure in both the fast and slow formations. The present study confirms that the two orthogonal dipole flexural dispersions are nearly parallel to each other in slow formations and nonintersecting in fast formations, even in deviated wellbores and in the presence of a sonic tool structure described by a heavy-fluid column.

INTRODUCTION

Deviated drilling through the overburden shale is often required to access horizontal wells in a reservoir. Large stress-induced shear anisotropy in the borehole cross-sectional plane can be an indicator of the potential instability for the chosen well deviation. Most of the sedimentary rocks exhibit some degree of anisotropy. A horizontally layered structure exhibits transversely isotropic (TI) anisotropy with a vertical (X_3-) axis of symmetry. A TI anisotropy is also referred to as polar anisotropy with five independent anisotropic moduli. The orientation of a deviated wellbore is defined by rotating the TI-anisotropy axes by angle θ about the X_1-axis in the isotropic plane. The rotated anisotropic constants referred to the borehole axes consists of nine nonzero, anisotropic moduli.

Analytical solutions of elastic-waves can be obtained only in a TI formation with its symmetry axis parallel to the borehole axis VTI (White and Tongtaow, 1981; Chan and Tsang, 1983; Ellefsen et al., 1991). Most of the anisotropic environments, including a TI formation with horizontal axis of symmetry (HTI), require the use of a perturbation technique or a numerical finite-difference time-domain (FDTD) formulation of the linear equations of motion in anisotropic materials (Wang and Tang, 2003). Sinha et al. (1994) proposed the use of an equivalent isotropic reference state in a perturbation model to account for an arbitrary state of formation anisotropy. It has also been demonstrated that a properly selected, equivalent isotropic state adequately accounts for most of the weakly anisotropic formations (Sinha and Zeroug, 1999; Thomsen, 1986). This choice of an equivalent isotropic reference state minimizes the amount of pertur-

Manuscript received by the Editor January 25, 2006; revised manuscript received July 5, 2006; published online November 3, 2006.
[1]Schlumberger-Doll Research, 36 Old Quarry Road, Ridgefield, Connecticut 06877. E-mail: bsinha@ridgefield.oilfield.slb.com.
[2]Duke University, Department of Electrical and Computer Engineering, Durham, North Carolina 27708. E-mail: esl@ee.duke.edu; qhliu@ee.duke.edu.

bative correction in the modal dispersions to account for the remaining formation structural anisotropy.

It is known that phase and group velocities of the three plane waves can be different for propagation in nonprincipal directions of anisotropic materials (Musgrave, 1970). It is also known that transient elastic-waves caused by acoustic emission, friction, and dislocation motion propagate at their group velocities. Kim and Sachse (1993) have demonstrated that a broadband point source and point receiver can be used to measure group velocities in a TI zinc crystal. They have experimentally confirmed that the detected pulse signal contains a compressional arrival at the first break, followed by a zero crossing, and a sharp trough indicating the two shear-wave arrivals at their corresponding group velocities. Processing algorithms designed to estimate moveouts of sharp discontinuities in a pulse would yield group velocities of the three plane waves for any nonprincipal propagation direction in anisotropic materials. It is therefore possible to estimate group velocities of the three plane waves from the recorded waveforms in deviated boreholes in highly anisotropic formations. When the processing of recorded waveforms estimates moveouts of the first break, the zero crossing, or a sharp crest or trough, we can obtain the corresponding group velocities of plane waves in anisotropic materials (Wang et al., 2002; Hornby et al., 2003).

In contrast, the slowness-time-coherence (STC) algorithm is designed to estimate phase velocity, or slowness of a coherent arrival, from an array of recorded waveforms (Kimball and Marzetta, 1984). Similarly, variations of Prony's algorithm (such as a modified matrix pencil algorithm) are designed to isolate both dispersive and nondispersive arrivals in the recorded wavetrain that estimate phase velocities or slownesses as a function of frequency from an array of recorded waveforms (Lang et al., 1987; Ekstrom, 1995).

This paper describes an FDTD formulation of elastic-wave propagation in a fluid-filled borehole in an arbitrarily anisotropic formation with 21 independent elastic moduli. Both monopole and dipole synthetic waveforms have been obtained in deviated boreholes in fast and slow TI formations. Processing of these waveforms with a modified matrix pencil algorithm (Ekstrom, 1995) yields modal dispersions, in terms of phase slowness as a function of frequency, associated with the Stoneley fast- and slow-dipole modes. The zero-frequency intercept of the Stoneley dispersion yields the tube-wave velocity, whereas low-frequency asymptotes of the fast- and slow-dipole dispersions correspond to the SH- and qSV-polarized shear-wave velocities. We compare phase velocities, or slownesses, obtained from our processing of synthetic waveforms with those from theoretical calculations of both the phase and group velocities of plane waves propagating in nonprincipal directions of anisotropic formations.

THEORY

The propagation of small-amplitude waves in homogeneous and anisotropic solids is described by the linear equations of motion. These equations can be written in Cartesian coordinates as

$$\tau_{\alpha\beta,\alpha} = \rho v_{\beta,t}, \tag{1}$$

$$\tau_{\alpha\beta,t} = C_{\alpha\beta\gamma\delta} v_{\gamma,\delta}, \tag{2}$$

where ρ is the formation mass density, $v_{j,t}$ is the particle acceleration, and $C_{\alpha\beta\gamma\delta}$ denotes the second-order elastic constant that satisfies the following symmetry relations:

$$C_{\alpha\beta\gamma\delta} = C_{\beta\alpha\gamma\delta} = C_{\beta\alpha\delta\gamma} = C_{\beta\gamma\delta\alpha}. \tag{3}$$

In all of these equations, we have used the Cartesian tensor notation and the convention that a comma followed by an index α (denotes differentiation with respect to X_α, and a comma followed by an index t denotes differentiation with respect to time. The Greek letters α, β, γ, and δ take on the values 1, 2, and 3. The summation convention for repeated tensor indices is implied also. Elastic plane waves can propagate along a given direction in an anisotropic solid in three distinct and mutually orthogonal modes in the absence of any degeneracy. These waves may not be either purely longitudinal or transverse in an arbitrarily anisotropic medium.

Most geophysical formations exhibit anisotropy that is characterized by TI symmetry. When referred to the principal axes of the material, there are five independent elastic constants for a TI solid. When the propagation direction is parallel to the TI symmetry axis, there is one longitudinal wave and there are two degenerate transverse waves that propagate with the same velocity. In contrast, when the propagation direction is perpendicular to the TI symmetry axis, there is one longitudinal wave and two distinct, mutually orthogonal, pure transverse waves with different velocities. However, when the propagation direction is obliquely inclined to the TI symmetry axis, as is the case in a deviated wellbore, the anisotropic medium supports a purely transverse (SH) and two mixed (qP and qSV) modes of plane waves.

There are two ways of obtaining the plane-wave solution for an arbitrary propagation direction in anisotropic materials: First, we can solve equation 1 with only five independent elastic moduli in the stiffness tensor C_{ijkl} but with an additional number of independent variables X_1 and X_3. A plane-wave solution in this approach can be expressed as

$$u_k = A_k \exp(i\omega n_j X_j / v), \tag{4}$$

where A_k is the normalized polarization vector, n_j denotes the direction cosines of the propagation vector with respect to the fixed anisotropy axes of the material, u_k is the particle displacement associated with the elastic-wave propagation with velocity v, and the subscripts k and j take on values 1, 2, and 3. Substituting this solution into equation 1, the plane-wave velocity is then given by

$$\rho v^2 = A_i A_k C_{ijkl} n_j n_l, \tag{5}$$

where ρ is the mass density. The polarization vector A_i is obtained from the solution of a 3×3 matrix eigenvalue problem, which is also known as the Kelvin-Christoffel equation (Fedorov, 1968; Musgrave, 1970; Norris and Sinha, 1993). We assume that the wavenormal n_j is parallel to the borehole axis. Second, we select the propagation direction parallel to the rotated X_3'-axis rotate the stiffness tensor C_{ijkl} to the new set of measurement axes and still work with only one independent variable X_3'. However, the rotated stiffness tensor referred to the deviated wellbore axes exhibits nine nonzero, elastic moduli that have to be accounted for in obtaining the wave solution. We use the second approach for obtaining the solution in the case of deviated wellbores. Figure 1 shows a schematic diagram of a vertical wellbore parallel to the X_3-axis and of a deviated wellbore with azimuth ϕ measured from north and with deviation θ measured from the vertical direction.

The rotated elastic stiffness tensor C'_{pqrs} is obtained from the following orthogonal transformation relations:

$$C'_{pqrs} = a_{pi}a_{qj}a_{rk}a_{sl}C_{ijkl}, \tag{6}$$

where a_{pi} is the rotation matrix that defines the orthogonal transformation between the two sets of axes and is given by

$$a_{pi} = \begin{bmatrix} \cos\phi & \sin\phi & 0 \\ -\cos\theta\sin\phi & \cos\theta\cos\phi & \sin\theta \\ \sin\theta\sin\phi & -\sin\theta\cos\phi & \cos\theta \end{bmatrix}, \tag{7}$$

where ϕ and θ are the Euler angles between the rotated axes (primed) and the reference anisotropy axes (unprimed). The angle ϕ denotes the rotation about the X_3-axis that defines the well azimuth, and θ denotes the rotation about the X_1-axis that defines the deviation angle.

When the elastic moduli (or stiffnesses) are specialized to the case of a TI anisotropy, they can be expressed in terms of a 6×6 matrix as given below:

$$\mathbf{C}_{ij} = \begin{bmatrix} C_{11} & C_{12} & C_{13} & 0 & 0 & 0 \\ & C_{11} & C_{13} & 0 & 0 & 0 \\ & & C_{33} & 0 & 0 & 0 \\ & & & C_{44} & 0 & 0 \\ & & & & C_{44} & 0 \\ & & & & & C_{66} \end{bmatrix}, \tag{8}$$

where $C_{66} = (C_{11} - C_{12})/2$ and we have used Voigt's compressed notation that combines the two indices into one using the following transformation: $(11 \rightarrow 1)$, $(22 \rightarrow 2)$, $(33 \rightarrow 3)$, $(23 \rightarrow 4)$, $(31 \rightarrow 5)$, and $(12 \rightarrow 6)$. When the TI elastic moduli are rotated by angle θ about the X_1-axis, with the rotated X_3-axis parallel to the deviated wellbore axis, the rotated elastic moduli for such a tilted TI formation take the form

$$\mathbf{C}_{ij} = \begin{bmatrix} C_{11} & C_{12} & C_{13} & C_{14} & 0 & 0 \\ & C_{22} & C_{23} & C_{24} & 0 & 0 \\ & & C_{33} & C_{34} & 0 & 0 \\ & & & C_{44} & 0 & 0 \\ & & & & C_{55} & C_{56} \\ & & & & & C_{66} \end{bmatrix}. \tag{9}$$

Norris and Sinha (1996) have shown that the presence of C_{14}, C_{24}, C_{34}, and C_{56} (referred to the rotated axes) in a tilted TI formation cause anisotropy-induced coupling between the quasi-Stoneley and quasi-flexural modes. However, these moduli affecting the coupling do not have any influence on the low-frequency limit of the quasi-Stoneley wave velocity. The low-frequency limit of the azimuthally symmetric Stoneley wave velocity, also referred to as the tube-wave velocity, in an isotropic formation is given by (White, 1983)

$$V_T = V_f\,(1 + K_f/\mu)^{-1/2}, \tag{10}$$

where V_f and K_f denote the borehole-fluid compressional velocity and bulk modulus, respectively, and μ is the formation shear modulus. Recently, this analytical expression for the tube-wave velocity has been extended to include weakly anisotropic formations (Norris and Sinha, 1996; Chi and Tang, 2004). It has been shown that the tube-wave velocity V_T in a weakly anisotropic formation can be expressed in terms of an effective shear modulus μ^* given by (Norris and Sinha, 1996)

$$\mu^* = (C_{11} + C_{22} - 2C_{12} + 4C_{66})/8. \tag{11}$$

This expression for the effective shear modulus is not restricted to any particular material symmetry and is equally valid for a triclinic or a TI formation. However, this result is derived for weakly anisotropic formations that include most of the sedimentary rocks that we encounter in the oil and gas industry (Thomsen, 1986). The shear modulus $C^*_{66} = \mu^*$ denotes shear rigidity in the borehole cross-sectional plane and can be substituted in equation 10 to obtain the tube-wave velocity in a general anisotropic formation.

The finite-difference formulation of equation 1 in 3D cylindrical coordinates applied to a fluid-filled borehole is described in detail by Liu and Sinha (2003). So we will now proceed to describe results from this FDTD formulation of the linear equations of motion.

COMPUTATIONAL RESULTS I: AUSTIN CHALK

The plane-wave velocities and associated polarization vectors are obtained from the solution of Kelvin-Christoffel equations for an arbitrary propagation direction from the TI symmetry axis. Table 1 contains the elastic constants and mass density of Austin Chalk used

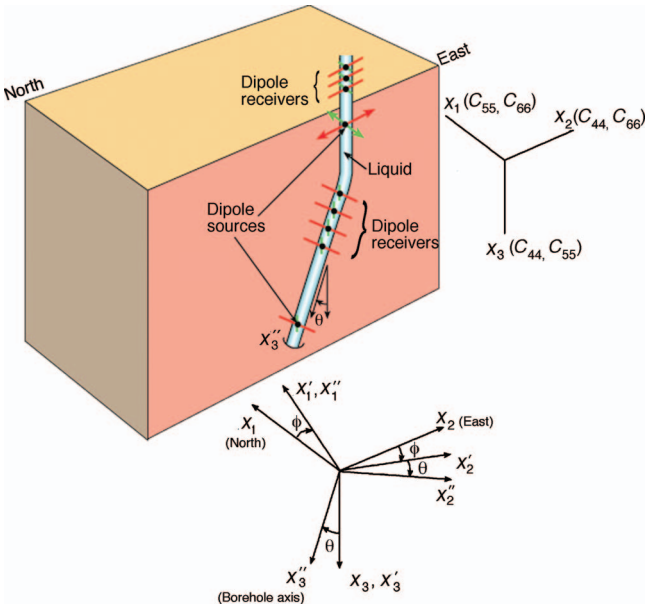

Figure 1. Schematic diagram of a vertical well parallel to the X_3-axis and a deviated well with azimuth ϕ and deviation θ.

Table 1. Model parameters.

Formation	ρ (kg/m^3)	C_{11} (N/m^2)	C_{12} (N/m^2)	C_{13} (N/m^2)	C_{33} (N/m^2)	C_{44} (N/m^2)
Austin Chalk	2200	22 E + 9	15.8 E + 9	12 E + 9	14 E + 9	2.4 E + 9
Cotton Valley Shale	2640	74.73 E + 9	14.75 E + 9	25.29 E + 9	58.84 E + 9	22.05 E + 9

in this study (White, 1983). The borehole fluid is assumed to have a compressional speed of 1500 m/s and mass density of 1000 kg/m^3. All computational results are for a borehole of radius 10.16 cm (4 inches). This formation is classified as a slow formation whose shear slowness is larger than the borehole-fluid compressional slowness. Because a TI material is invariant with respect to any rotation about the symmetry axis (or equivalently, about the well azimuth in a formation with a vertical TI symmetry axis), we show in Figure 2a and b, respectively, the tube-wave velocity and qP-, qSV-, and SH-wave velocities as a function of well deviation θ from the TI symmetry axis. The solid and dashed curves, respectively, denote the phase and group velocities in Figure 2a and b. Differences between the phase and group velocities of the qP- and SH-waves are largest for propagation directions ranging from 30° to 60° from the TI symmetry axis. In contrast, larger differences between the phase and group velocities of the qSV-wave occur for propagation directions ranging from 10° to 30° and from 50° to 80° from the symmetry axis. Notice that the tube-wave velocity in Figure 2b changes by only about 3% over the entire range of wellbore deviations, whereas shear- and compressional-wave velocities change by up to about 12%–25%, respectively.

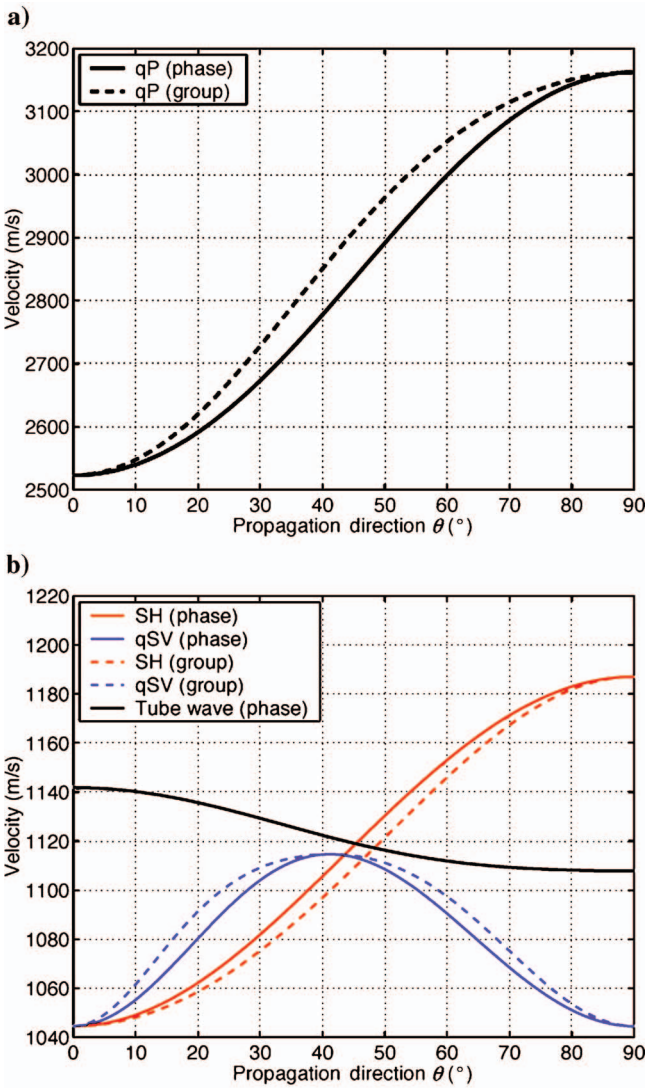

Figure 2. (a) The solid and dashed lines, respectively, denote the qP-wave phase and group velocities as a function of propagation direction from the TI-symmetry axis in a slow Austin Chalk Formation. The propagation direction coincides with the wavenormal direction from the TI-symmetry axis. (b) The black curve denotes the tube wave velocity as a function of propagation direction from the TI-symmetry axis in a slow Austin chalk formation. The solid and dashed curves, respectively, represent the phase and group velocities of qSV- and SH-waves as a function of propagation direction from the TI-symmetry axis in a slow Austin Chalk Formation.

Elastic moduli versus well deviation

The bottom inset in Figure 1 shows the cross-sectional plane X_1''-X_2'' of a deviated wellbore with azimuth ϕ and deviation θ. A dipole source oriented along the X_1''-direction generates borehole flexural waves propagating along the X_3''-axis corresponding to the SH-wave whose velocity is largely dependent on the rotated shear modulus C_{55} in the X_1''-X_3'' plane.

Variations of plane-wave velocities follow the same trend as the dominant elastic moduli that appear as the diagonal elements in the elastic stiffness matrix. Figure 3a and b, respectively, displays variations in the elastic moduli C_{22} and C_{33} and in C_{44}, C_{55}, and C_{66} as a function of wellbore deviations. The compressional velocity along the deviated wellbore is largely dependent on the variation of C_{33}, whereas the SH-wave velocity is dependent on the variation of C_{55} with the deviation angle. The qSV-wave and tube-wave velocities are dependent on certain combinations of elastic moduli. However, the qSV-wave and tube-wave velocities follow the trend of the elastic moduli C_{44} and C_{66}, respectively, as shown in Figure 3b.

Norris and Sinha (1995, 1996) have shown that the Stoneley and dipole flexural modes are coupled when the elastic moduli C_{14}, C_{24}, C_{34}, and C_{56}, referred to the deviated wellbore axes, are significantly large. This coupling can give rise to processing challenges in situations when the borehole Stoneley and flexural dispersions are close.

Austin Chalk: Wellbore deviation 0°

When the wellbore deviation is 0°, elastic-waves propagate parallel to the TI-symmetry axis, and the phase and group velocities coincide. Figure 4a shows synthetic waveforms at an array of receivers produced by a monopole source placed on the borehole axis. These waveforms are processed by a modified matrix pencil algorithm to isolate both dispersive and nondispersive arrivals in the wavetrain (Lang et al., 1987; Ekstrom, 1995). Figure 4b displays the monopole compressional slowness and Stoneley dispersion in a fluid-filled wellbore in the absence of any tool structure. The dashed blue lines denote analytical results for the tube-wave S_T and the qP-wave phase slownesses. The low-frequency Stoneley dispersion agrees very well with the analytical result for the tube-wave phase slowness S_T for this configuration.

Figure 5a displays synthetic waveforms at an array of receivers produced by a dipole source placed on the borehole axis and oriented along the X_2''-axis in the deviated borehole cross-sectional plane. The low-frequency asymptote of this borehole flexural wave coincides with the qSV-wave velocity. The qSV-wave polarization vector is in the $X_2 - X_3''$ plane, and the qSV-wave velocity is largely dependent on the rotated shear modulus C_{44} in the $X_2'' - X_3''$ plane. There are two packets of coherent arrivals. The first is the dipole compressional mode, and the second is the borehole flexural mode. Figure 5b shows the flexural and dipole compressional dispersions obtained after processing the waveforms shown in Figure 5a. The dashed blue lines denote analytical results for the SH- and qP-wave slownesses. The

low-frequency asymptote of flexural dispersion agrees very well with the analytical solution of the qSV-wave phase slowness obtained from the solution of the Kelvin-Christoffel equations.

Austin Chalk: Wellbore deviation 60°

Next, we analyze our results from a wellbore with a deviation of 60° from the vertical; the propagation direction of elastic-waves in such a wellbore is 60° from the TI symmetry axis. We show in Figure 6a synthetic waveforms at an array of receivers produced by a dipole source placed on the borehole axis and oriented parallel to the qSV-wave polarization direction. The first coherent arrival is a dipole compressional mode, and the second one is the lowest-order borehole flexural mode. Figure 6b displays the flexural and dipole compressional dispersions obtained after processing the waveforms shown in Figure 6a. The dashed blue lines denote analytical results for the qSV- and qP-wave phase slownesses for a wavenormal coincident with the well deviation angle. The solid blue line indicates the corresponding group slowness of the qP-wave. The group slowness (327.6 μs/m) is slightly smaller than the phase slowness (333.5 μs/m) for this deviated wellbore. Notice that the extracted qP-wave slowness coincides with the calculated phase slowness. The low-frequency asymptote of flexural dispersion agrees very well with the analytical solution of the qSV-wave slowness for this wellbore deviation of 60°.

Figure 7a shows synthetic waveforms at an array of receivers produced by a dipole source placed on the borehole axis and oriented parallel to the SH-wave polarization direction. Because the wave propagation is 60° from the TI-symmetry axis, the qSV- and SH-waves travel with different velocities. We display in Figure 7b, the borehole flexural and dipole compressional slownesses, as a function of frequency, obtained from the processing of the synthetic waveforms in Figure 7a. The dashed blue lines denote analytical results for the SH- and qP-wave phase slownesses. Again, the low-fre-

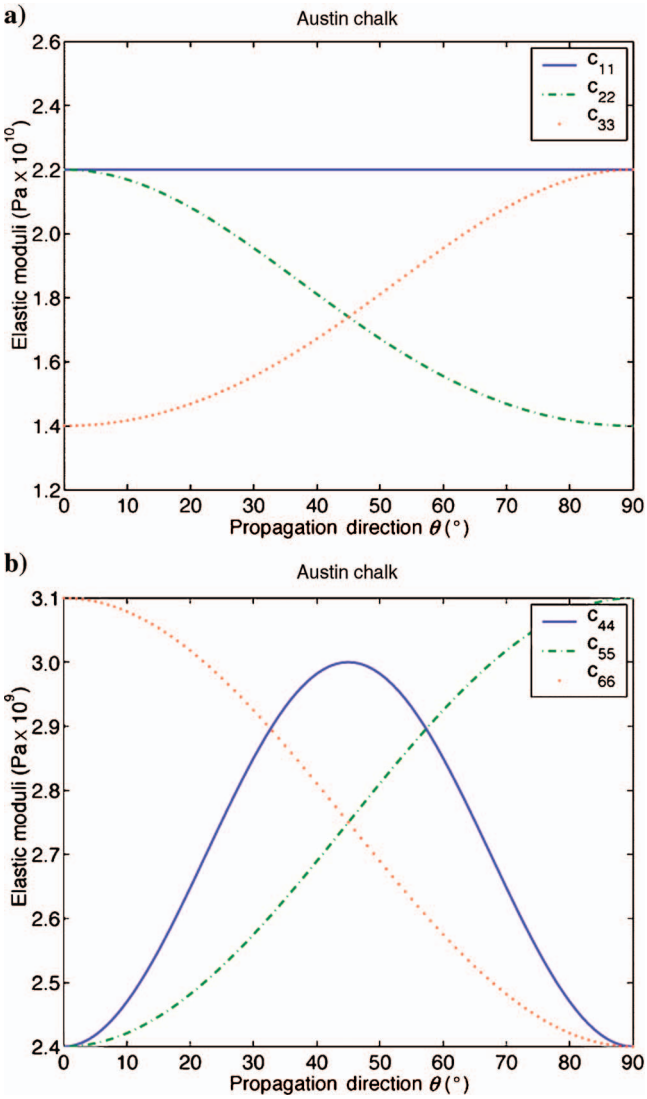

Figure 3. (a) Elastic moduli C_{22} and C_{33} (in pascals) as a function of propagation direction from the TI-symmetry axis in a slow Austin Chalk Formation. The modulus C_{11} = 2.2 E + 10 Pa, is a constant for rotation about the X_1-axis. (b) Elastic moduli C_{44}, C_{55}, and C_{66} (in pascals) as a function of propagation direction from the TI symmetry axis in a slow Austin Chalk Formation.

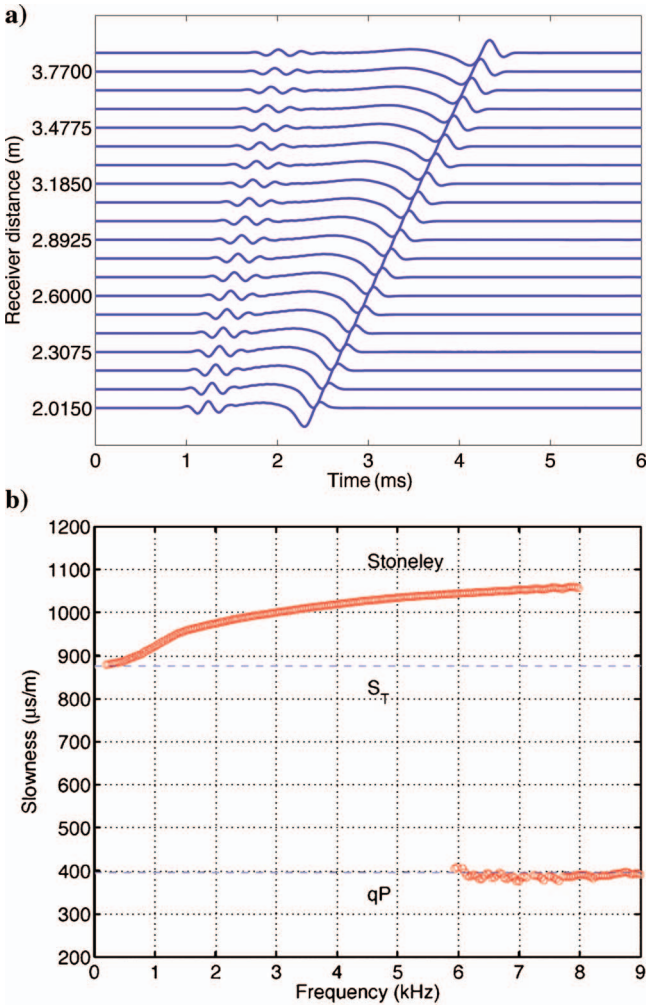

Figure 4. (a) Synthetic waveforms produced by a monopole source placed on the borehole axis parallel to the TI symmetry axis in a slow Austin Chalk Formation in the absence of any tool structure. (b) Monopole compressional slowness and Stoneley dispersion obtained from synthetic waveforms shown in Figure 4a. Results are for propagation parallel to the TI symmetry axis in a slow Austin Chalk Formation.

quency asymptote of the flexural dispersion agrees very well with the SH-wave slowness obtained from the solution of the Kelvin-Christoffel equations for this wellbore deviation of 60°.

Sonic tool effects on borehole dispersions in slow formations

Next, we describe the influence of a sonic tool structure on elastic-waves in a fluid-filled borehole in anisotropic formations (Pistre et al., 2005). The influence of this sonic tool structure on borehole dispersions is described by a heavy-fluid column placed concentrically with the borehole axis. To study the influence of the tool structure on the monopole Stoneley mode, we introduce a heavy-fluid column of the same diameter as the tool structure and its mass density as the mean density of the tool. The compressional velocity of the heavy fluid is estimated from calibrating this model parameter to properly account for the tool bias as a function of the wellbore diameter and formation compressional velocity. However, the influence of the tool structure on the borehole flexural mode is adequately accounted for in terms of a fixed, heavy-fluid compressional velocity and the same heavy-fluid column diameter and mass density as that for the monopole Stoneley mode. The heavy-fluid column is introduced as an additional cylindrical member in the FDTD formulation with appropriate parameters for the monopole and dipole waves.

Austin Chalk: Wellbore deviation 30°

Figure 8a–c, respectively, compares the monopole Stoneley and dipole compressional, and flexural dispersions in the absence (red circles) and in presence (blue crosses) of a heavy-fluid column with calibrated parameters to account for the sonic tool structure bias on sonic data. The dashed blue lines in Figure 8a–c denote analytical results for the tube-wave, qP-, qSV-, and SH-wave phase slownesses. These results are for elastic-wave propagation in a deviated wellbore

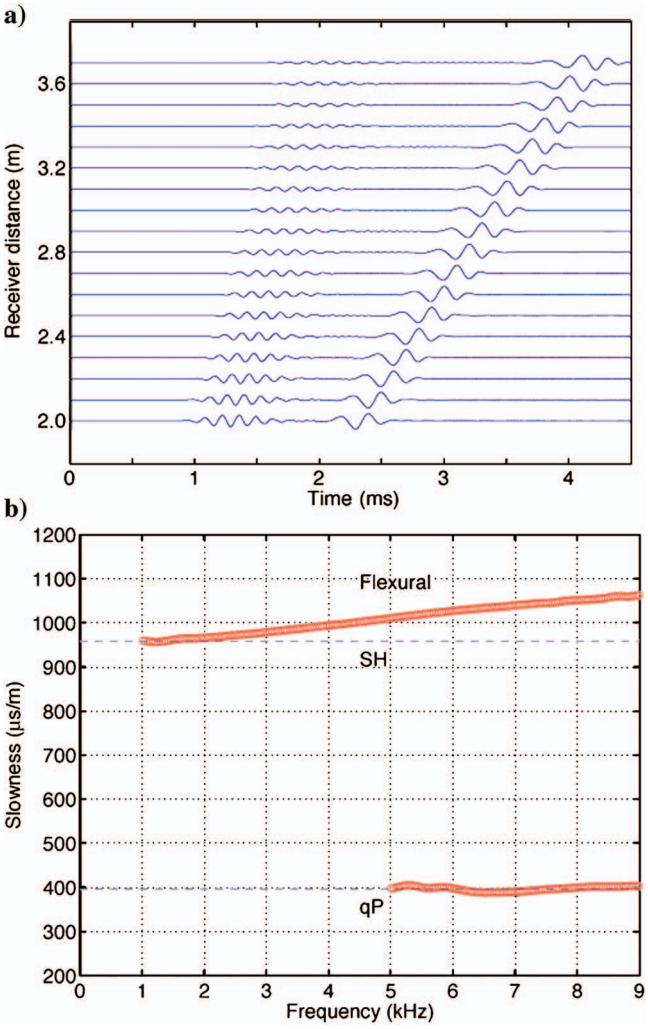

Figure 5. (a) Synthetic waveforms produced by a dipole source placed on the borehole axis parallel to the TI symmetry axis in a slow Austin Chalk Formation in the absence of any tool structure. Dipole orientation is parallel to the SH-wave polarization. (b) Dipole compressional slowness and borehole flexural dispersion obtained from synthetic waveforms shown in Figure 5a. Results are for propagation parallel to the TI symmetry axis in a slow Austin Chalk Formation.

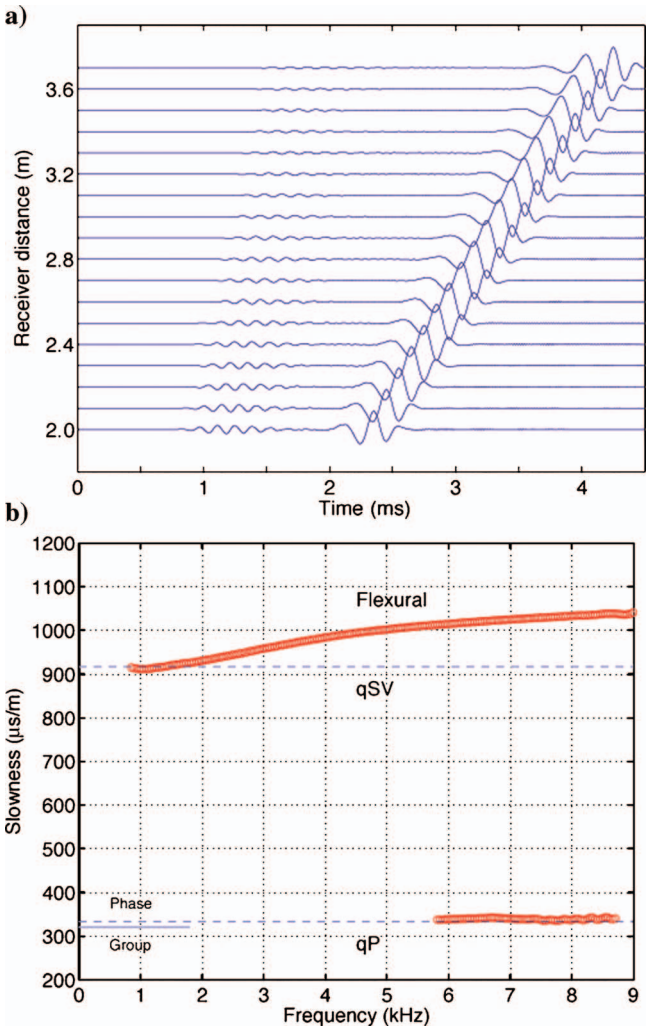

Figure 6. (a) Synthetic waveforms produced by a dipole source placed on the borehole axis in a 60° deviated wellbore in a slow Austin Chalk Formation. Dipole orientation is parallel to the qSV-wave polarization. (b) Dipole compressional and borehole flexural dispersion obtained from synthetic waveforms shown in Figure 6a. Results are for propagation in a 60° deviated wellbore in a slow Austin Chalk Formation.

(deviation = 30°). First, we notice that the nondispersive part of the dipole compressional wave is not affected by the tool presence. Second, the borehole flexural dispersion also is not affected by the tool presence in this slow Austin chalk formation. However, we observe that the monopole Stoneley dispersion is affected by the tool presence at low frequencies and not affected at high frequencies.

Next, we provide a composite plot of monopole and dipole dispersions obtained in a 30° deviated borehole using a monopole and two orthogonal dipole transmitters. Figure 9a shows borehole dispersions in the absence of any tool structure. The solid and dashed lines, respectively, denote the phase and group slownesses for the qP-, qSV-, and SH-waves. Clearly, low-frequency asymptotes of flexural dispersions coincide with the corresponding phase slownesses of shear waves. Similarly, the extracted qP-wave slowness agrees with the computed phase slowness using the Kelvin-Christoffel equations. Notice that the fast and slow dipole dispersions corresponding to the SH- and qSV-waves are nearly parallel to each other as predicted by a previously reported perturbation analysis (Sinha et al., 1994). Figure 9b displays the monopole Stoneley and dipole flexural dispersions in the presence of an equivalent heavy-fluid column to describe the tool bias on borehole dispersions. The notation is the same as in Figure 9a. Even though there is a discernible difference in the Stoneley dispersion shown in Figure 9a in the absence of any tool structure to that shown in Figure 9b in the presence of an equivalent heavy-fluid column, the fast and slow dipole dispersions are nearly parallel. Consequently, nonintersecting dipole dispersions are indicators of formation intrinsic anisotropy, whereas crossing dipole dispersions are indicators of stress-induced anisotropy dominating the sonic data (Sinha and Kostek, 1996). Interestingly, the dipole compressional slowness is not affected by the presence of this tool structure. Both the inline and crossline dipole transmitters produce compressional head waves with essentially the same compressional slowness shown in Figure 9a and b.

COMPUTATIONAL RESULTS II: COTTON VALLEY SHALE

Generally, borehole waves in fast formations propagate with larger amplitude over a wider bandwidth than those in slow formations. Unlike slow formations, the monopole Stoneley mode is a normal mode at all frequencies and is strongly excited in fast formations. Sonic tool effects described in terms of a heavy-fluid column with calibrated parameters are also larger in fast formations.

Next, we calculate the plane-wave velocities and associated polarization vectors from the solution of the Kelvin-Christoffel equations for an arbitrary propagation direction from the TI symmetry axis. Table 1 contains the elastic constants and mass density of Cotton Valley Shale used in this study (Thomsen, 1986). The shear slowness of a fast formation is smaller than the borehole-liquid compressional slowness. Because a TI material is invariant with respect to any rotation about the symmetry axis (or equivalently, about the well azimuth in a formation with a vertical TI symmetry axis), we show in Figure 10a–c, respectively, the qP-, tube-wave velocity, and qSV- and SH-wave velocities as a function of well deviation θ from the TI symmetry axis. Notice that the tube-wave velocity changes by only about 1.5% over the entire range of wellbore deviations, whereas shear- and compressional-wave velocities change by up to about 10% to 15%, respectively.

Elastic moduli versus well deviation

We show in Figure 11a and b, respectively, variations in the elastic moduli C_{22} and C_{33}, and C_{44}, C_{55}, and C_{66} as a function of wellbore deviation in a fast Cotton Valley Shale Formation. As is the case with a slow Austin Chalk Formation, the compressional velocity along the deviated wellbore is largely dependent on the variation of C_{33} and increases with increasing deviation angle. Similarly, the SH-wave velocity is dependent on the variation of C_{55} with the deviation angle, and it also increases with increasing deviation angle. Even though the qSV-wave velocity is dependent on certain combinations of elastic moduli, the variation of qSV-wave phase velocity with the deviation angle follows the same trend as that of the dominant elastic modulus C_{44} with the wellbore deviation. Likewise, the tube-wave velocity is also dependent on a combination of elastic moduli. However, the variation of tube-wave phase velocity as a function of wellbore deviation shown in Figure 10b also is remarkably similar to the variation of the modulus C_{66} with the propagation direction.

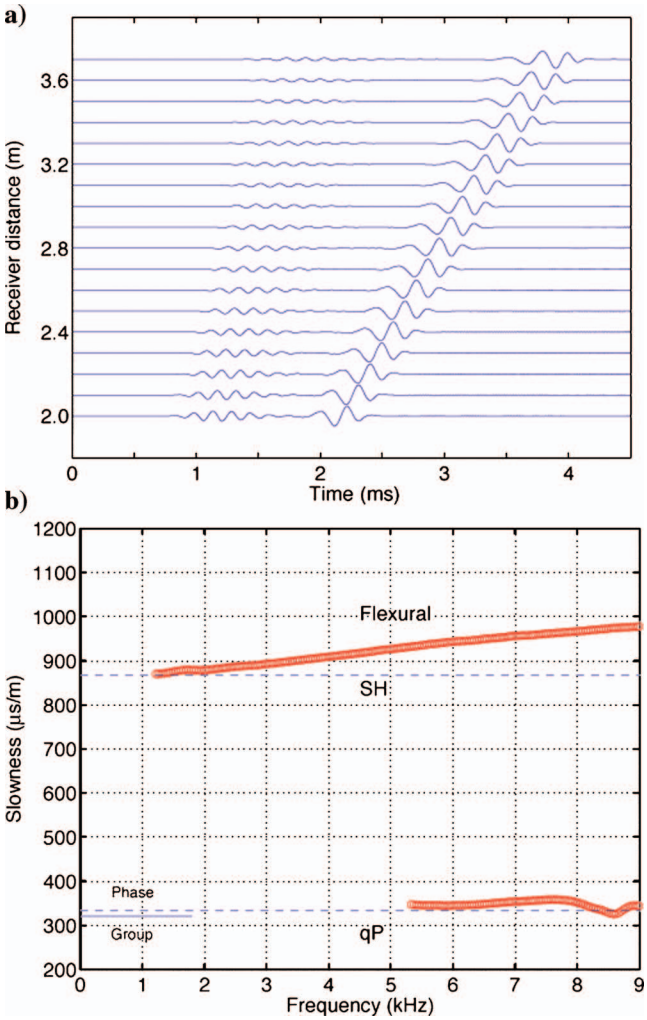

Figure 7. (a) Synthetic waveforms produced by a dipole source in a 60° deviated wellbore in a slow Austin Chalk Formation in the absence of any tool structure. Dipole orientation is parallel to the SH-wave polarization. (b) Dipole compressional and borehole flexural dispersions obtained from synthetic waveforms shown in Figure 7a. Results are for propagation in a 60° deviated wellbore in a slow Austin Chalk Formation.

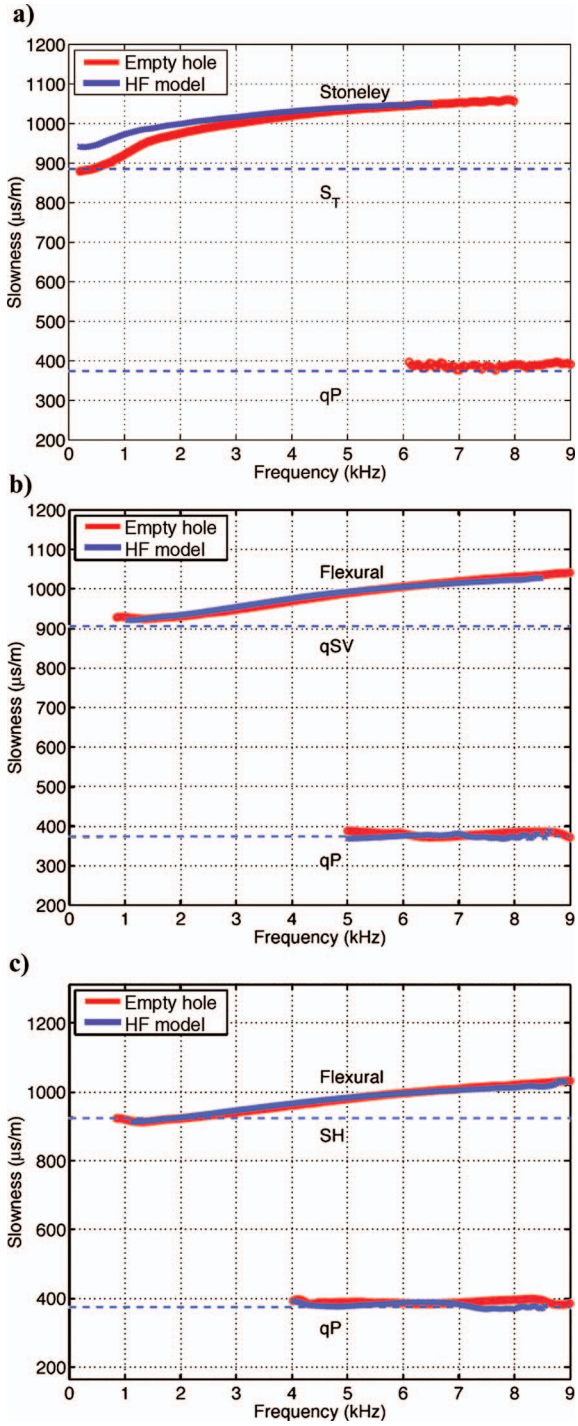

Figure 8. (a) Comparison of the monopole Stoneley dispersion in a fluid-filled borehole in the absence (red circles) and in the presence of an equivalent heavy-fluid (HF) column to describe the tool bias on measured data (solid blue curve). Wellbore deviation is 30°. (b) Comparison of the dipole compressional and qSV-flexural dispersions in a fluid-filled borehole in the absence (red curve) and in the presence of an equivalent heavy-fluid column to describe the tool bias on measured data (blue curve). Wellbore deviation is 30°. (c) Comparison of the dipole compressional and SH flexural dispersions in a fluid-filled borehole in the absence (red curve) and in the presence of an equivalent heavy-fluid column to describe the tool bias on measured data (blue crosses). Wellbore deviation is 30°. Dashed lines denote phase slownesses for the SH- and qP-waves.

Norris and Sinha (1996) have shown that the Stoneley and dipole flexural modes are coupled for propagation in nonprincipal directions in a TI formation. The elastic moduli C_{14}, C_{24}, C_{34}, and C_{56} become nonzero with respect to the measurement axes, as is the case in deviated wellbores.

Sonic tool effects on borehole dispersions in fast formations

Generally, the influence of a sonic tool structure on elastic-waves in a fluid-filled borehole is larger in faster formations and in smaller borehole diameters than in slower formations and larger boreholes. Although the low-frequency asymptotes of flexural dispersions are not affected by the tool presence, the Stoneley dispersion is affected

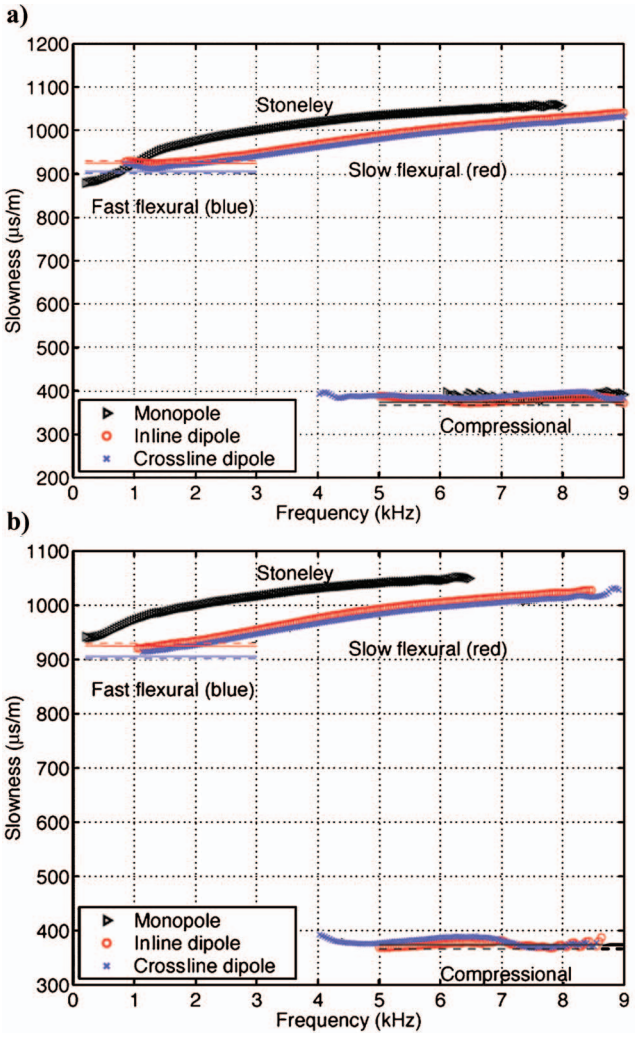

Figure 9. (a) Monopole Stoneley and dipole dispersions and dipole compressional slowness in a 30° deviated borehole in the absence of any tool structure. The fast and slow shear waves correspond to the SH-and qSV-waves propagating along the borehole. The solid and dashed lines, respectively, denote the phase and group slownesses for the qP-, qSV-, and SH-waves.(b) Monopole Stoneley and dipole flexural dispersions and dipole compressional slowness in a 30° deviated borehole in the presence of a heavy-fluid column to account for tool effects on borehole dispersions. The solid and dashed lines, respectively, denote the phase and group slownesses for the qSV- and SH- waves.

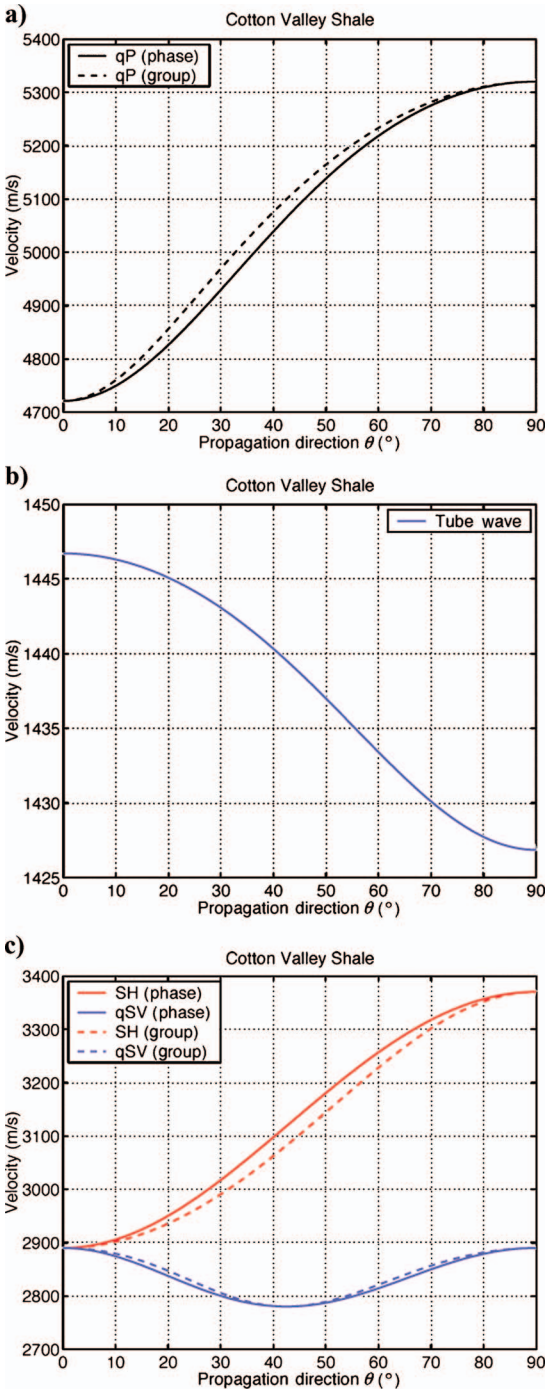

Figure 10. (a) The solid and dashed lines, respectively, denote the qP (compressional) phase and group velocities as a function of propagation direction from the TI symmetry axis in a fast Cotton Valley Shale Formation. The propagation direction coincides with the wavenormal direction from the TI symmetry axis. (b) Tube wave phase velocity as a function of propagation direction from the TI symmetry axis in a fast Cotton Valley Shale Formation. (c) The solid and dashed lines, respectively, denote the phase and group velocities of the qSV- and SH- waves as a function of propagation direction from the TI symmetry axis in a fast Cotton Valley Shale Formation. The propagation direction coincides with the wavenormal direction from the TI symmetry axis.

by the presence of any tool structure at all frequencies. To study the influence of the tool structure, we use an equivalent heavy-fluid column placed concentrically with the borehole axis with the same heavy-fluid parameters as in the case of slow formations. As before, the compressional velocity of the heavy fluid is selected by calibrating this model parameter to properly account for the tool bias on the borehole Stoneley dispersion as a function of the wellbore diameter and formation compressional velocity.

Cotton Valley Shale: Wellbore deviation 90°

When the wellbore deviation is 90°, elastic-waves propagate perpendicular to the TI symmetry axis. Figure 12a shows synthetic waveforms at an array of receivers produced by a monopole source placed on the borehole axis in the absence of any tool structure. These waveforms are processed by a modified matrix pencil algorithm to isolate both dispersive and nondispersive arrivals in the wavetrain.

Figure 12b compares the monopole Stoneley and pseudo-Rayleigh dispersions in the absence (red circles) and in the presence (blue crosses) of a heavy-fluid column with calibrated parameters to account for the tool structure bias on sonic data. These results are for elastic-wave propagation perpendicular to the TI symmetry axis

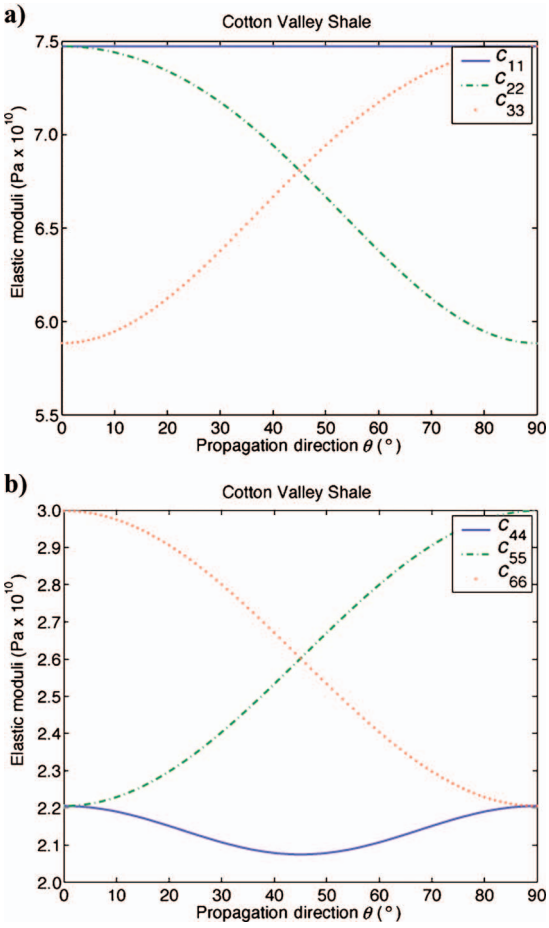

Figure 11. (a) Elastic moduli C_{11} (or C_{22}) and C_{33} (in Pa) as a function of propagation direction from the TI symmetry axis in a fast Cotton Valley Shale Formation. (b) Elastic moduli C_{44}, C_{55}, and C_{66} (in Pa) as a function of propagation direction from the TI symmetry axis in a fast Cotton Valley Formation.

(wellbore deviation 90°) in a fast Cotton Valley Shale Formation. Because this is one of the principal propagation directions, both the phase and group slownesses of all plane waves coincide. We observe that the monopole Stoneley dispersion is significantly affected by the tool presence at all frequencies in fast formations. However, the nondispersive part of the pseudo-Rayleigh mode is not affected much by the tool presence as shown in Figure 12b. The low-frequency Stoneley dispersion or the tube-wave phase slowness agrees very well with the analytical result for this propagation direction in the absence of any tool structure. The low-frequency asymptote of the pseudo-Rayleigh mode also agrees well with the SH-wave phase slowness for this propagation direction.

Figure 13a displays synthetic waveforms at an array of receivers produced by a dipole source placed on the borehole axis perpendicular to the TI symmetry axis and oriented along the SH-wave polarization in the absence of any tool structure. There are two packets of coherent arrivals. The first is the direct shear head wave followed by a dispersive borehole flexural mode. Figure 13b compares the lowest-order flexural mode and a higher-order flexural mode that merges with the shear head wave slowness at low frequencies in the absence (red circles) and in the presence (blue crosses) of a heavy-fluid column with calibrated parameters to account for the tool structure bias on sonic data. These results are for elastic-wave propagation perpendicular to the TI symmetry axis (wellbore deviation 90°) in a fast Cotton Valley Shale Formation. We observe that the borehole flexural dispersion is significantly affected by the tool presence in this fast Cotton Valley Shale Formation except at very low frequencies as shown in Figure 13b. However, the nondispersive SH head wave in this fast formation is not affected by the tool presence as is evident from Figure 13b. The low-frequency asymptote of flexural dispersion agrees very well with the analytical solution for the SH-wave phase slowness obtained from the solution of the Kelvin-Christoffel equations.

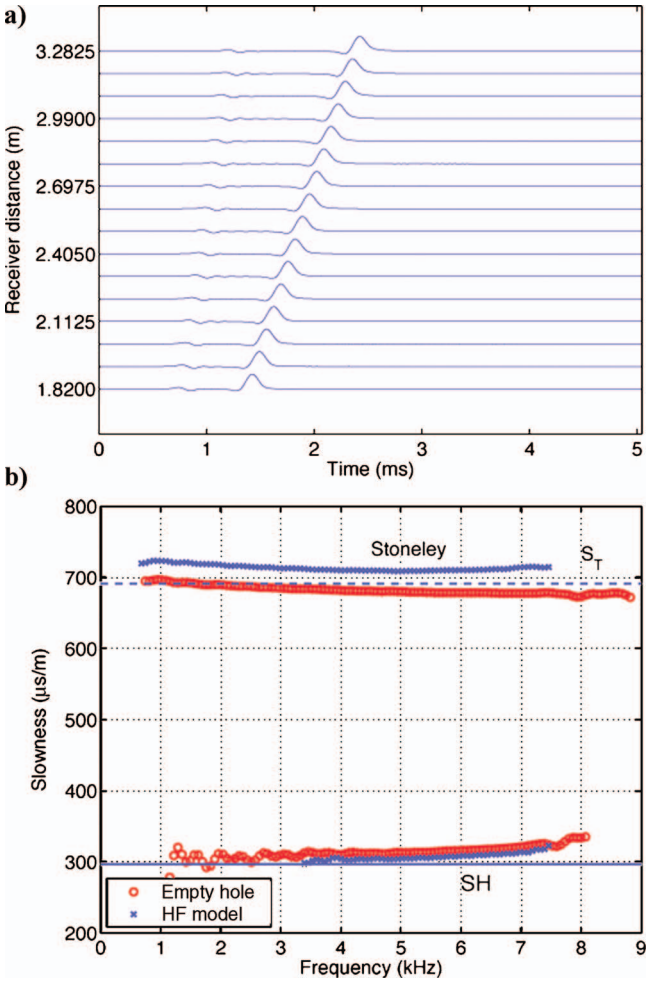

Figure 12. (a) Synthetic waveforms produced by a monopole source on the borehole axis perpendicular to the TI symmetry axis in a fast Cotton Valley Shale Formation in the absence of any tool structure. (b) Monopole pseudo-Rayleigh and Stoneley dispersions obtained from synthetic waveforms in the absence (red circles) and in the presence (blue crosses) of a heavy-fluid column to account for the tool effects. Results are for propagation perpendicular to the TI symmetry axis in a fast Cotton Valley Shale Formation.

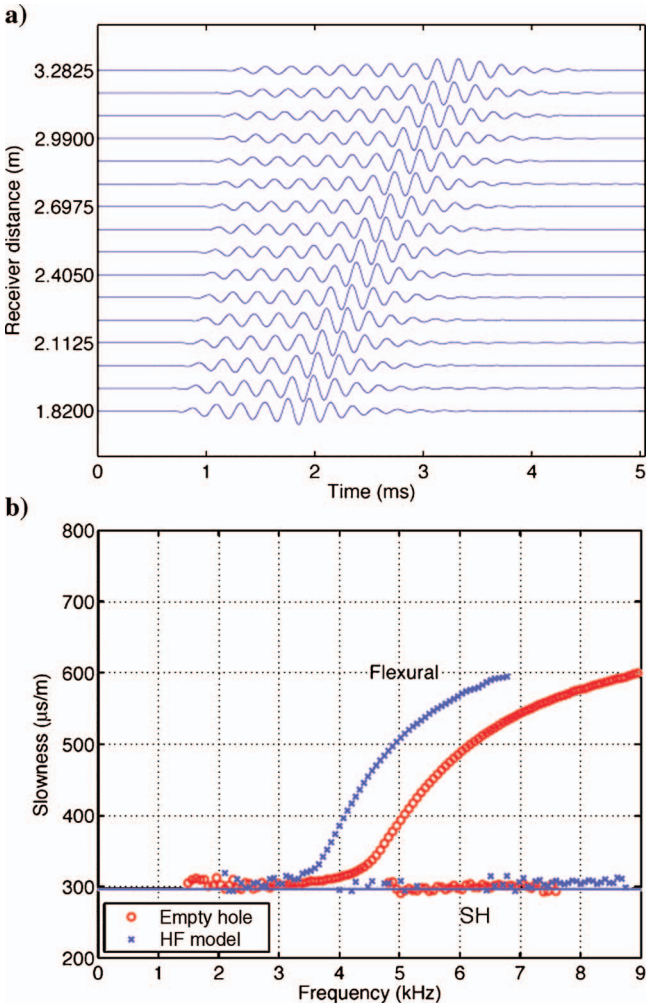

Figure 13. (a) Synthetic waveforms produced by a dipole source placed on the borehole axis perpendicular to the TI symmetry axis in a fast Cotton Valley Shale Formation in the absence of any tool structure. Dipole orientation is parallel to the SH-wave polarization. (b) Dipole shear head wave and borehole flexural dispersion obtained from synthetic waveforms in the absence (red circles) and in the presence (blue crosses) of a heavy-fluid column to account for the tool effects. Results are for propagation perpendicular to the TI symmetry axis in a fast Cotton Valley Shale Formation.

Cotton Valley Shale: Wellbore deviation 30°

Next we analyze our results from a wellbore with a deviation of 30° from the TI symmetry axis. Figure 14a shows synthetic waveforms at an array of receivers produced by a monopole source placed on the borehole axis in the absence of any tool structure. These waveforms are also processed by a modified matrix pencil algorithm to isolate both dispersive and nondispersive arrivals in the wavetrain.

Figure 14b compares the monopole Stoneley and pseudo-Rayleigh dispersions in the absence (red circles) and in the presence (blue crosses) of a heavy-fluid column with calibrated parameters to account for a sonic tool structure bias on sonic data. These results are for elastic-wave propagation 30° from the TI symmetry axis (wellbore deviation 30°) in a fast Cotton Valley Shale Formation. The dashed blue line (S_T) denotes the tube-wave phase slowness for this propagation direction. Notice that the monopole Stoneley dispersion is significantly affected by the tool presence at all frequencies in deviated wellbores. However, the nondispersive part of the pseudo-Rayleigh mode is not affected much by the tool presence, as shown in Figure 14b. The solid and dashed blue lines (SH) represent the phase and group slownesses for the SH-wave. Notice that the group slowness for this propagation direction is larger than the phase slowness as shown in Figure 10c. The low-frequency Stoneley dispersion agrees very well with the analytical result for the tube-wave slowness for this configuration. The low-frequency pseudo-Rayleigh dispersion coincides with the analytical result for the SH-wave phase slowness.

Figure 15a displays synthetic waveforms at an array of receivers produced by a dipole source placed on the borehole axis and oriented parallel to the SH-wave polarization direction in the absence of any

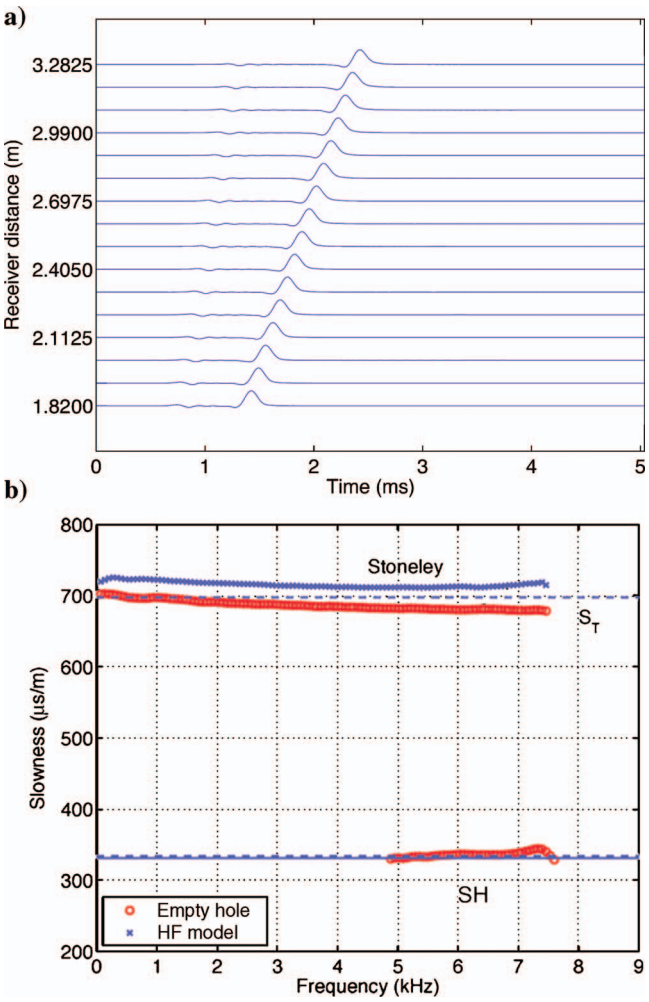

Figure 14. (a) Synthetic waveforms produced by a monopole source in a wellbore deviated 30° from the TI symmetry axis in a fast Cotton Valley Shale Formation in the absence of any tool structure. (b) Comparison of the monopole Stoneley and pseudo-Rayleigh dispersions in a fluid-filled borehole in the absence (red circles) and in the presence (blue crosses) of an equivalent heavy-fluid column to describe the tool bias on measured data. Wellbore deviation is 30°. The solid and dashed blue lines, respectively, denote the phase and group slownesses for the SH-wave propagating at 30° from the TI symmetry axis.

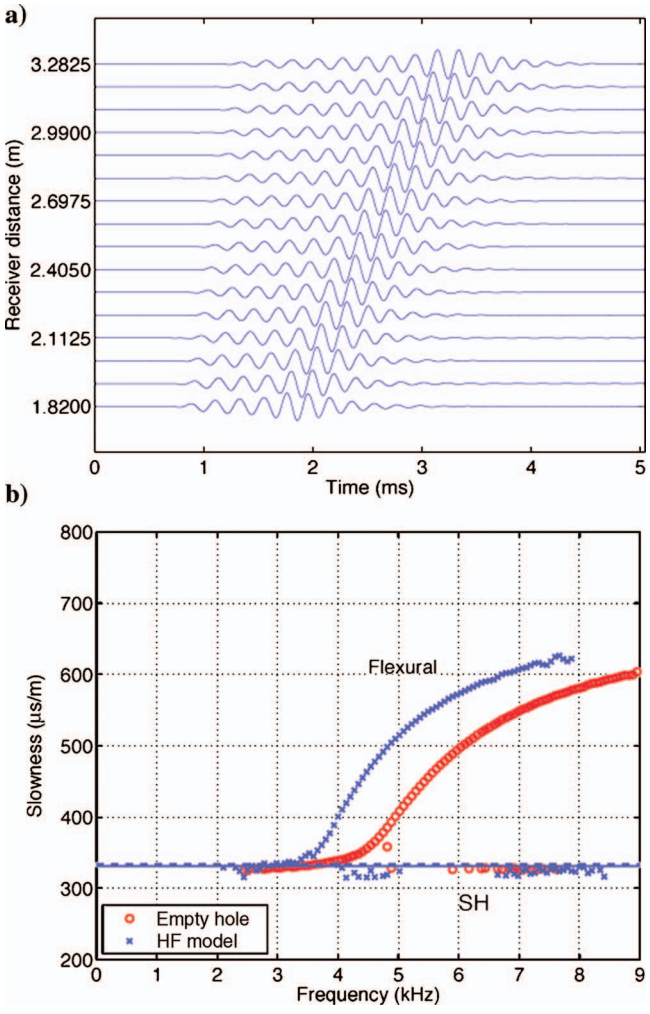

Figure 15. (a) Synthetic waveforms produced by a dipole source in a 30° deviated wellbore in a fast Cotton Valley Shale Formation in the absence of any tool structure. Dipole orientation is parallel to the SH-wave polarization. (b) Comparison of the SH-wave phase slowness and SH flexural dispersion in a fluid-filled borehole in the absence (red circles) and in the presence (blue crosses) of an equivalent heavy-fluid column to describe the tool bias on measured data. Wellbore deviation is 30°. The solid and dashed blue lines, respectively, denote the phase and group slownesses for the SH-wave propagating at 30° from the TI symmetry axis.

tool structure. There are two packets of coherent arrivals. The first is a nondispersive SH head wave followed by a dispersive borehole flexural mode.

Figure 15b compares the lowest-order flexural dispersion and a higher-order flexural mode whose low-frequency slowness coincides with the SH-wave phase slowness in the absence (red circles) and in the presence (blue crosses) of a heavy-fluid column with calibrated parameters to account for a sonic tool structure bias on sonic data. The solid and dashed blue lines (SH) represent analytical results for the phase and group slownesses for the SH-wave propagating at 30° from the TI symmetry axis (wellbore deviation 30°) in a fast Cotton Valley Shale Formation. Notice that the borehole flexural dispersion is significantly affected by the tool presence in this fast Cotton Valley Shale Formation except at very low frequencies as shown in Figure 15b. However, the nondispersive SH head wave slowness is not affected by the tool presence.

CONCLUSIONS

We have used a 3D cylindrical FDTD with PML formulation of the linear equations of motion in arbitrarily anisotropic materials to study the influence of a sonic tool structure on elastic-wave propagation in a fluid-filled borehole in both TI and tilted TI formations. A tilted TI formation refers to a wellbore with dipping beds or to a deviated wellbore with its axis obliquely inclined with respect to the TI symmetry axis. Phase and group velocities of the three plane waves can be different for propagation along deviated wellbores in anisotropic formations. Processing of synthetic waveforms in deviated wellbores using a conventional STC algorithm or a modified matrix pencil algorithm yields phase slownesses of the compressional and shear waves propagating in the nonprincipal directions of anisotropic formations. This has been confirmed by comparing the processed results with theoretical results for the phase and group slownesses (or velocities) for plane waves propagating along arbitrary directions in anisotropic formations. However, it is also possible to extract group slownesses or velocities of plane waves by monitoring moveouts of sharp discontinuities or crests of the propagating pulse. Therefore, we conclude that different processing algorithms can be used to extract either phase or group velocities from an array of recorded waveforms excited by a broadband pulse.

Even though an FDTD formulation is expected to yield all coherent arrivals supported by the surrounding formation, we observe that weaker arrivals are not easily detected by processing the synthetic waveforms using the modified matrix pencil algorithm. In particular, we did not see any evidence of anisotropy-induced coupling between the Stoneley and dipole modes in deviated wellbores in either the fast or slow TI formations. Earlier calculations of the degree of anisotropy-induced coupling to the Stoneley mode produced by a dipole source in a 60° deviated wellbore in Austin Chalk indicate that the magnitude of Stoneley amplitude is −20 to −30 dB below the flexural amplitude. Signals that are so much smaller than the peak amplitude are not detected with the FDTD formulation together with the processing algorithm used in this study.

Computational results for the Stoneley dispersion show negligibly small changes consistent with small changes in the tube-wave velocity for different wellbore deviations. In contrast, cross-dipole dispersions exhibit relatively larger changes consistent with the qSV- and SH-wave velocities as a function of wellbore deviation.

The fast- and slow-dipole dispersions are nearly parallel in a slow TI formation for different well deviations. These results are consistent with predictions from a previously reported perturbation analysis results.

The influence of this sonic tool structure is negligibly small on both the monopole pseudo-Rayleigh mode in fast formations and on dipole compressional slownesses in slow formations. It is important to note that the fast and slow dipole dispersions remain nearly parallel even in the presence of a heavy-fluid column as an equivalent model for the sonic tool structure at hand.

ACKNOWLEDGMENTS

The authors thank the associate editor Vladimir Grechka and anonymous reviewers for many constructive comments and suggestions.

REFERENCES

Chan, A. K., and T. Tsang, 1983, Propagation of acoustic waves in a fluid-filled borehole surrounded by a concentrically layered transversely isotropic formation: Journal of the Acoustical Society of America, **74**, 1605–1616.

Chi, S., and X. M. Tang, 2004, Stoneley wave speed modeling in general anisotropic formations: 74th Annual International Meeting, SEG, Expanded Abstracts, 338–341.

Ekstrom, M. E., 1995, Dispersion estimation from borehole acoustic arrays using a modified matrix pencil algorithm: Proceedings of the 29th Asilomar Conference on Signals, Systems and Computers, IEEE Computer Society, 449–453.

Ellefsen, K. J., C. H. Cheng, and M. N. Toksoz, 1991, Effects of anisotropy upon the normal modes in a borehole: Journal of the Acoustical Society of America, **89**, 2597–2616.

Fedorov, F. I., 1968, Theory of elastic-waves in crystals: Plenum Press.

Hornby, B., X. Wang, and K. Dodds, 2003, Do we measure phase or group velocity with dipole sonic tools?: 65th Annual Meeting, EAGE, Paper F29.

Kim, K. Y., and W. Sachse, 1993, Determination of all elastic constants of transversely isotropic media with a cusp around the symmetric axis by use of elastic pulses propagating in two principal directions: Physical Review B, **47**, 10993–11000.

Kimball, C. V., and T. M. Marzetta, 1984, Semblance processing of borehole acoustic array data: Geophysics, **49**, 264–281.

Lang, S. W., A. L. Kurkjian, J. H. McClellan, C. F. Morris, and T. W. Parks, 1987, Estimating slowness dispersion from arrays of sonic logging waveforms: Geophysics, **52**, 530–544.

Liu, Q. H., and B. K. Sinha, 2003, A 3D cylindrical PML/FDTD method for elastic-waves in fluid-filled pressurized boreholes in triaxially stressed formations: Geophysics, **68**, 1731–1743.

Musgrave, M. J. P., 1970, Crystal acoustics: Holden-Day.

Norris, A. N., and B. K. Sinha, 1993, Weak elastic anisotropy and the tube wave: Geophysics, **58**, 1091.

———, 1995, The speed of a wave along a fluid/solid interface in the presence of anisotropy and prestress: Journal of the Acoustical Society of America, **98**, 1147–1154.

———, 1996, Anisotropy-induced coupling in borehole acoustic modes: Journal of Geophysical Research, **101** (B7), 15945–15952.

Pistre, V., T. Kinoshita, T. Endo, K. Schilling, J. Pabon, B. Sinha, T. Plona, T. Ikegami, and D. Johnson, 2005, A modular wireline sonic tool for measurements of 3D (azimuthal, radial, and axial) formation acoustic properties: Presented at the 46th Annual Logging Symposium, Society of Professional Well Logging Analysts.

Sinha, B. K., and S. Kostek, 1996, Stress-induced azimuthal anisotropy in borehole flexural waves: Geophysics, **61**, 1899–1907.

Sinha, B. K., A. N. Norris, and S. K. Chang, 1994, Borehole flexural modes in anisotropic formations: Geophysics, **59**, 1037–1052.

Sinha, B. K., and S. Zeroug, 1999, Geophysical prospecting using sonics and ultrasonics, *in* John G. Webster, ed., Wiley Encyclopedia of Electrical and Electronics Engineering: Wiley Interscience, 340–365.

Thomsen, L., 1986, Weak elastic anisotropy: Geophysics, **51**, 1954–1966.

Wang, X., B. Hornby, and K. Dodds, 2002, Dipole sonic response in deviated boreholes penetrating an anisotropic formation: 72nd Annual Meeting, SEG, Expanded Abstracts, 360–363.

Wang, X., and X. Tang, 2003, Finite-difference modeling of elastic-wave propagation: A non-splitting perfectly matched layer approach: Geophysics, **68**, 1749–1755.

White, J. E., 1983, Underground Sound: Elsevier Science Publ. Co., Inc.

White, J. E., and C. Tongtaow, 1981, Cylindrical waves in transversely isotropic media: Journal of the Acoustical Society of America, **70**, 1147–1155.